RSC Advances

PAPER

View Article Online
View Journal | View Issue

Cite this: *RSC Adv.*, 2016, **6**, 65252

High performance hybrid graphene–$CsPbBr_{3-x}I_x$ perovskite nanocrystal photodetector†

Do-Hyun Kwak, Da-Hye Lim, Hyun-Soo Ra, Parthiban Ramasamy and Jong-Soo Lee*

Received 5th April 2016
Accepted 29th June 2016

DOI: 10.1039/c6ra08699c

www.rsc.org/advances

We demonstrate a highly sensitive hybrid photodetector based on graphene–$CsPbBr_{3-x}I_x$ perovskite nanocrystals. This hybrid photodetector exhibits a high photo-responsivity of $\sim 10^8$ A W^{-1} and detectivity of $\sim 10^{16}$ jones at an irradiance power of 0.07 μW cm^{-2} under 405 nm illumination.

Introduction

Colloidal quantum dots, well known as semiconductor nanocrystals (NCs), have been of interest in optoelectronic applications because of their size dependent bandgap, strong light-absorbing property, versatile surface architecture with various functional ligands, and easy fabrication of large-area films.[1–5] Recently, metal halide perovskites have exhibited remarkable potentials for photovoltaic, light emitting diode, and photodetector applications.[6–8] Hybrid organic–inorganic lead halide perovskites $MAPbX_3$ (X = Cl, Br, I) have received much attention by exhibiting rapid increase of power conversion efficiency up to 20% in photovoltaic devices.[6] More recently, all inorganic cesium lead halide ($CsPbX_3$, X = Cl, Br, I) perovskite NCs exhibited high quantum yield up to 90%. In addition, the bandgap of $CsPbX_3$ perovskite NCs can easily tuned by anion exchange reactions at room temperature.[9–11] In photodetector application, the organometallic halide perovskite device demonstrated the responsivity of $\sim$0.4 A W^{-1} and detectivity of 10^{12} jones.[12] The $CsPbX_3$ NCs also exhibited a remarkable photocurrent on/off ratio of 10^5 as a promising absorption layer.[13] However, the photodetectors based on NCs have been suffered from the low carrier mobility of NCs films.[5]

In this respect, graphene having very high carrier mobility ($\sim$200 000 cm^2 V^{-1} s^{-1}) is hybridized with NCs to enhance the charge transport.[14] Many studies on hybridization between graphene and semiconductor NCs were reported as high performance photodetectors.[15–23] The hybrid photodetector of graphene and PbS quantum dots well known as intrinsically optoelectronic NCs exhibited the very high photo-responsivity of $\sim 10^7$ A W^{-1} with covering broad wavelength spectrum.[15] The hybrid graphene–organic lead halide perovskite photodetector exhibited high photo-responsivity of $\sim 10^6$ A W^{-1}.

Herein, we report hybrid graphene–$CsPbBr_{3-x}I_x$ NCs photodetector with highly photosensitivity. The hybrid photodetector results in a responsivity as high as 8.2×10^8 A W^{-1} and detectivity of 2.4×10^{16} jones at incident power of 0.07 μW cm^{-2} under 405 nm illumination. These results clearly demonstrate the potential of graphene–$CsPbBr_{3-x}I_x$ NCs photodetector for optoelectronic applications.

Results and discussion

Fig. 1a shows the schematic diagram of the hybrid graphene–$CsPbBr_{3-x}I_x$ photodetector. The hybrid photodetector was fabricated using a bilayer graphene mechanically exfoliated from the graphene flakes on the Si/SiO_2 substrate. Source–drain electrodes were patterned by electron beam lithography, and Ti

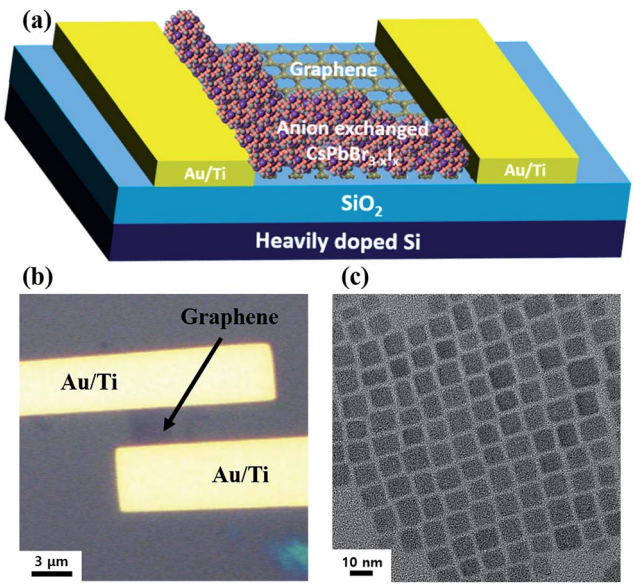

Fig. 1 (a) Schematic diagram of graphene–$CsPbBr_{3-x}I_x$ NCs photodetector. (b) Optical image of graphene device. (c) TEM image of anion exchanged $CsPbBr_{3-x}I_x$ NCs.

Department of Energy Systems Engineering, DGIST, Daegu 711-873, Republic of Korea. E-mail: jslee@dgist.ac.kr

† Electronic supplementary information (ESI) available. See DOI: 10.1039/c6ra08699c

of 5 nm and Au of 45 nm were deposited by using electron beam evaporation. Fig. 1b shows the optical image of the hybrid photodetector used in this study. The bilayer graphene shown in Fig. S1a† was confirmed by Raman spectroscopy. AFM image in Fig. S1b† illustrated the $CsPbBr_{3-x}I_x$ NCs were deposited uniformly on the graphene device. The $CsPbBr_{3-x}I_x$ NCs used in this study were obtained *via* anion exchange method, which previously was reported by our group.[13] The green emitting $CsPbBr_3$ NCs were synthesized and treated with LiI to form $CsPbBr_{3-x}I_x$ NCs. The $CsPbBr_{3-x}I_x$ NCs have bright red luminescence with a peak centered at 604 nm in Fig. S2b.† The $CsPbBr_{3-x}I_x$ NCs have cubic crystal structure as inferred from the X-ray diffraction (XRD) patterns in Fig. S2a† and cube morphology with size about 10 nm in Fig. 1c.

Fig. 2a shows the transfer curve at 1 V_{DS} (drain–source voltage) as a function of V_{GS} (gate–source voltage) for pristine graphene and graphene–$CsPbBr_{3-x}I_x$ NCs photodetector under dark and illumination, respectively. In the transfer curve, the Dirac point of pristine graphene device is located at 16 V_{GS} due to oxidation in fabrication of the graphene device as typically exhibiting p-type doping behavior. In graphene device, the variation of the Dirac point is originated from the doping behavior. After deposition of the $CsPbBr_{3-x}I_x$ NCs on graphene device, the Dirac point of the graphene was negatively shifted from 16 to −48 V_{GS} as exhibiting n-type doping behavior. This variation of the Dirac point of the hybrid graphene device is attributed to electron transfer from $CsPbBr_{3-x}I_x$ NCs (higher Fermi level) to graphene (lower Fermi level) in order to satisfy the equilibrium condition at the interface of the hybrid device. Here, the built-in field formed by the contact of two different materials gives rise to the barrier and favorable path for electron and hole transfer from $CsPbBr_{3-x}I_x$ NCs to graphene, respectively.

Under 405 nm illumination at incident power of 13.5 μW cm^{-2}, the Dirac point of graphene moves to the higher value of −25 V_{GS}. The shift of the Dirac point is attributed to the transport of carriers photogenerated from the NCs under illumination. The holes are transferred from $CsPbBr_{3-x}I_x$ NCs to graphene, and the electrons are trapped by the barrier formed by the band bending. Thus, doping effect in the hybrid device by the illumination leads to positive photocurrent ($I_p = I_{light} - I_{dark}$) for $V_{GS} \ll V_{Dirac}$ and negative photocurrent ($I_p = I_{dark} - I_{light}$) for $V_{GS} \gg V_{Dirac}$, respectively. This entire process is depicted in the schematic Fig. 2b–d.

Here, the Dirac point shifted by incident light in the hybrid device depends on optical power density. Fig. 3a shows the transfer curve as a function of gate–source voltage with varying optical power density. By increasing the incident power density,

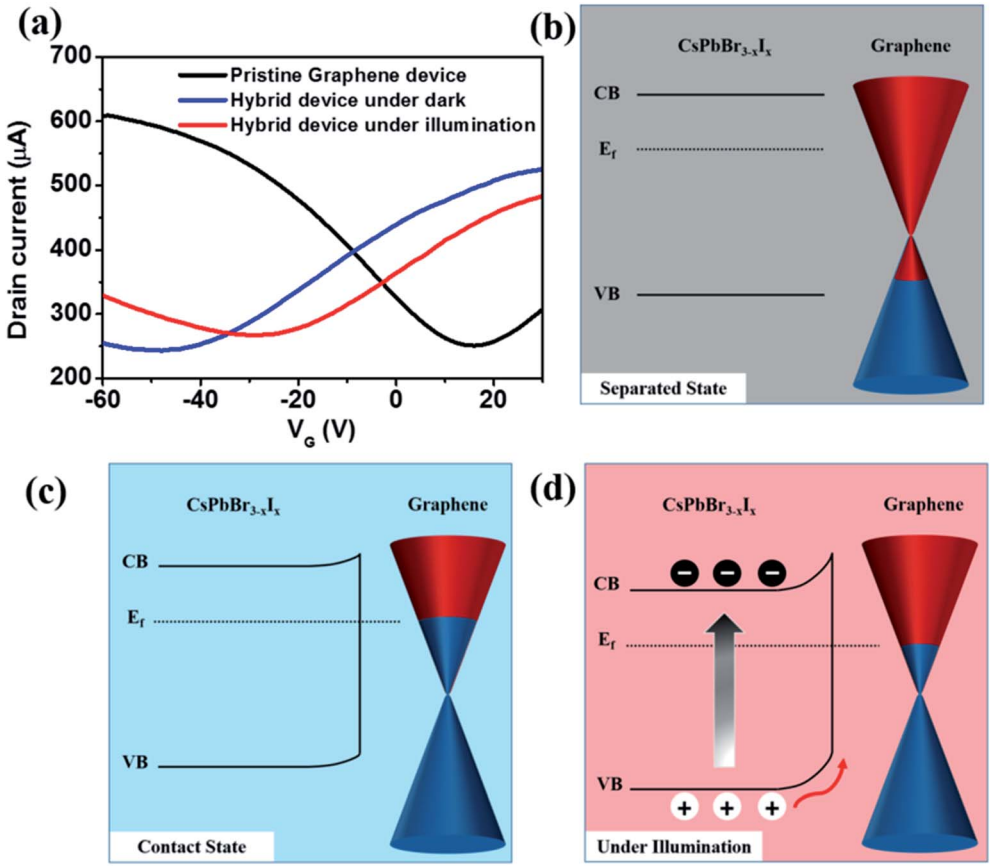

Fig. 2 (a) Transfer curve of graphene device and graphene–$CsPbBr_{3-x}I_x$ NCs photodetector under dark and illumination. (b) Energy diagram of graphene–$CsPbBr_{3-x}I_x$ NCs photodetector in the separated state. (c and d) Energy diagrams of graphene–$CsPbBr_{3-x}I_x$ NCs photodetector in contact state under dark (left) and illumination (right).

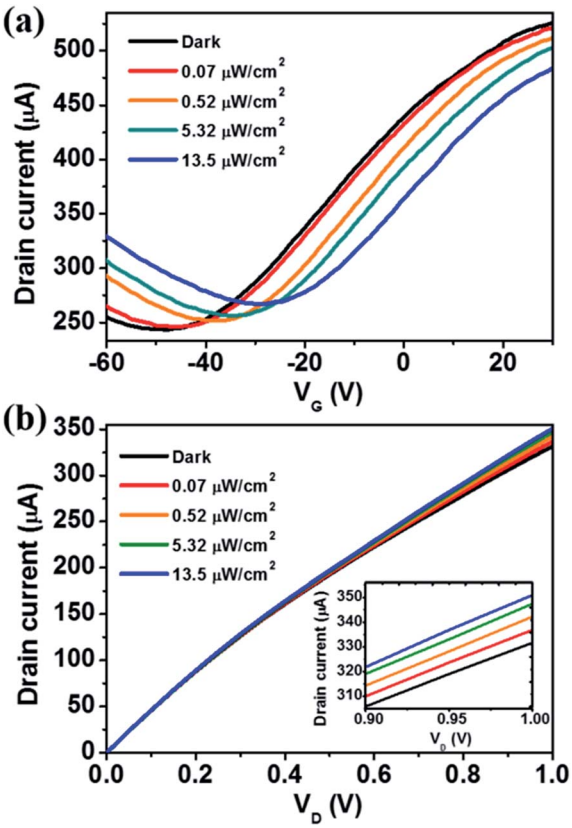

Fig. 3 (a) Transfer curve of graphene–$CsPbBr_{3-x}I_x$ NCs photodetector as a function of gate–source voltage at 1 V_{DS} with varying optical powers. (b) Output curve of graphene–$CsPbBr_{3-x}I_x$ NCs photodetector as a function of drain–source voltage at −60 V_{GS} with different optical powers. Inset shows the magnified portion of the output curve in range from 0.9 to 1.0 V_{DS}.

the Dirac point of the graphene moves to more positive value by leading to the higher photocurrent. Numbers of electron–hole pairs generated by the higher power density result in the high photocurrent in the graphene–$CsPbBr_{3-x}I_x$ NCs photodetector. In Fig. 3b, the output curve as a function of drain–source voltage at −60 V_{GS} with different optical powers becomes higher with increasing the optical power density. In order to make clear view of the output curve, a magnified portion from 0.9 to 1.0 V is shown in the inset.

The responsivity (R), as a figure of merit in photodetector, is calculated from the definition of $R = I_p/P$, where P is incident power, and I_p is the photocurrent measured at 1 V_{DS} in the output curve. Fig. 4a shows the responsivity of the hybrid device under 405 nm illumination with different optical power densities. The 0D–2D hybrid photodetectors usually have higher photoresponsivity than that of photodetectors based on NCs due to high mobility of 2D materials. Many literatures have reported highly photosensitive photodetectors based on graphene. Konstantatos *et al.* have reported PbS quantum dot (QD)–graphene photodetector with responsivity of $\sim 10^7$ A W^{-1}.[15] Guo *et al.* have reported ZnO QD–graphene photodetector with responsivity of 10^4 A W^{-1}.[18] Recently, the organic perovskite–graphene photodetectors have exhibited high responsivity of $\sim 10^6$ A W^{-1} and 180 A W^{-1}, respectively.[16,17] In the comparison, our hybrid photodetector shows the high responsivity ($\sim 10^8$ A W^{-1}) than the previous reports.

Another figure of merit in photodetector is detectivity (D^*) to characterize the optical signal which is of interest. We assumed that the short noise from direct current (DC) is the major contributor to the noise, and calculated the detectivity of the hybrid device as following equation of $D^* = (RA^{1/2})/(2qI_d)^{1/2}$, where A is active area of the device, e is the electron charge, and I_{dark} is dark current of the device.[24,25] The calculated specific detectivity of the hybrid device is up to 2.4×10^{16} jones in Fig. 4a. The detectivity of graphene–$CsPbBr_{3-x}I_x$ NCs photodetector exhibit three orders of magnitude higher than that of previous reported QDs photodetectors about $\sim 10^{13}$ jones.[4,26,27] The high detectivity of graphene–$CsPbBr_{3-x}I_x$ NCs photodetector is attributed to the rapid carrier transport of graphene and strong light absorbing property of $CsPbBr_{3-x}I_x$ NCs.

Fig. 4b shows the spectral photocurrent (black dot) of the graphene–$CsPbBr_{3-x}I_x$ NCs photodetector and absorption spectra (blue line) of $CsPbBr_{3-x}I_x$ NCs as a function of the wavelength. We used the $CsPbBr_{3-x}I_x$ NCs having first absorption peak centered at 584 nm as a light-absorbing material in our hybrid device. The photoresponse of the graphene–$CsPbBr_{3-x}I_x$ NCs photodetector in Fig. 4b matches with the absorption spectra of $CsPbBr_{3-x}I_x$ NCs as exhibiting the photocurrent peak at 580 nm. The spectral sensitivity of the hybrid photodetector based on graphene solely rely on the optical property of NCs because of weak light absorption of graphene. In this regard, the $CsPbX_3$ NCs could be more beneficial for hybrid photodetectors, because the absorption spectrum of $CsPbX_3$ NCs can be easily tuned over the entire visible ranges *via* anion exchange method at room temperature. The hybrid graphene–$CsPbBr_{3-x}I_x$ NCs photodetector can be used as building blocks for high efficiency and tunable selectivity in the visible range.

Fig. 4c shows the photocurrent–time (I_{ph}–t) response of the hybrid graphene–$CsPbBr_{3-x}I_x$ NCs photodetector measured in the dark and under illumination using a laser diode at 405 nm as a function of light intensity at fixed applied bias of 1 V under −60 V_G. The photocurrent of the hybrid device significantly increased with increasing of irradiance power showing good on-off switching behavior. The stability for photoresponse of the hybrid device are confirmed in Fig S3.† As shown in Fig. 4d, the rise and decay time calculated from the device using a single exponential function was 0.81 s and 3.65 s, respectively. The slow rise and decay time of the hybrid photodetector can be originated from the blockage of carrier transport due to the long-chain organic ligands on $CsPbBr_{3-x}I_x$ NCs. Short ligands can offer the rapid charge transport from NCs to graphene.[15,21] Replacing long ligands to short ligands, however, is highly difficult in graphene–$CsPbBr_{3-x}I_x$ NCs photodetector because the $CsPbX_3$ NCs are easily dissolved in polar solvents. Therefore, it is necessary to study on highly functional ligands for rapid charge transfer from NCs to graphene in order to improve the performance of 0D–2D hybrid photodetectors.

In conclusion, we demonstrated highly photosensitive $CsPbBr_{3-x}I_x$ NCs based photodetector, employing graphene as a transport layer. The hybridization between $CsPbBr_{3-x}I_x$ NCs

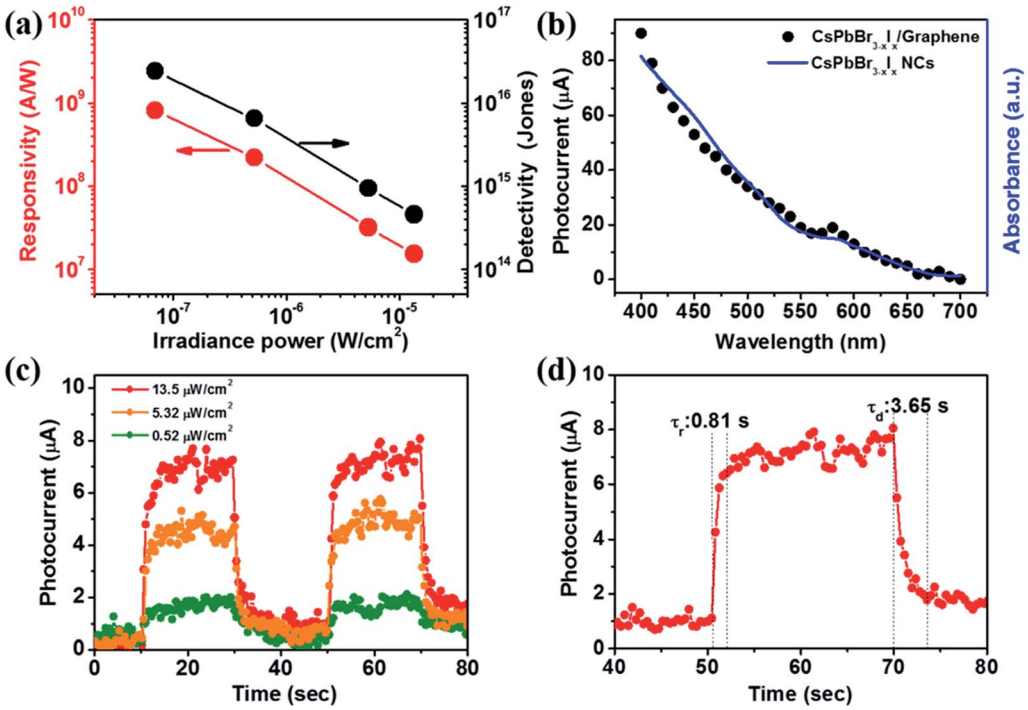

Fig. 4 Responsivity (R) and detectivity (D^*) of graphene–$CsPbBr_{3-x}I_x$ NCs photodetector for different irradiance powers under a wavelength of 405 nm at bias 1 V_{DS} and −60 V_{GS}. (b) Photocurrent in graphene–$CsPbBr_{3-x}I_x$ NCs photodetector (black dot) and absorbance in NCs as a function of spectral wavelength (blue line). (c) Temporal response of graphene–$CsPbBr_{3-x}I_x$ NCs photodetector for on/off illumination at bias 1 V_{DS} and −60 V_{GS}. (d) Temporal photocurrent response exited at illumination power of 13.5 μW cm^{-2}. Rise time (τ_r) and decay time (τ_d) are few seconds.

and graphene exhibited high photosensitivity due to the rapid carrier transport of the graphene. The responsivity of the hybrid graphene–$CsPbBr_{3-x}I_x$ NCs photodetector is 8.2×10^8 A W^{-1} at irradiance power of 0.07 μW cm^{-2} under 405 nm illumination. However, the slow rise and decay time (few seconds) of the graphene–$CsPbX_3$ NCs photodetector remain the severe bottleneck in photodetector application. In order to improve the rise and decay time, further studies will focus on the understanding of ligand effects in the hybrid graphene–quantum dot devices.

Acknowledgements

This work was supported by the DGIST R&D Program of the Ministry of Science, ICT and Future Planning (15-BD-0401) and the Leading Foreign Research Institute Recruitment Program (Grant No. 2012K1A4A3053565) through NRF funded by MEST. This work was partially supported by the Ministry of Trade, Industry & Energy of Korea (No. 10052853). We also thank H. S. Jang, S. K. Jeon (CCRF in DGIST) for discussions of Electron beam- and Photo-lithography system. Nano-device fabrication was carried out in clean room of CCRF.

References

1 E. H. Sargent, *Nat. Photonics*, 2012, **6**, 133–135.
2 Y. Shirasaki, G. J. Supran, M. G. Bawendi and V. Bulović, *Nat. Photonics*, 2012, 7, 13–23.
3 G. Konstantatos, I. Howard, A. Fischer, S. Hoogland, J. Clifford, E. Klem, L. Levina and E. H. Sargent, *Nature*, 2006, **442**, 180–183.
4 J. S. Lee, M. V. Kovalenko, J. Huang, D. S. Chung and D. V. Talapin, *Nat. Nanotechnol.*, 2011, **6**, 348–352.
5 D. V. Talapin, J.-S. Lee, M. V. Kovalenko and E. V. Shevchenko, *Chem. Rev.*, 2009, **110**, 389–458.
6 W. S. Yang, J. H. Noh, N. J. Jeon, Y. C. Kim, S. Ryu, J. Seo and S. I. Seok, *Science*, 2015, **348**, 1234–1237.
7 L. Dou, Y. M. Yang, J. You, Z. Hong, W. H. Chang, G. Li and Y. Yang, *Nat. Commun.*, 2014, **5**, 5404.
8 Z. K. Tan, R. S. Moghaddam, M. L. Lai, P. Docampo, R. Higler, F. Deschler, M. Price, A. Sadhanala, L. M. Pazos, D. Credgington, F. Hanusch, T. Bein, H. J. Snaith and R. H. Friend, *Nat. Nanotechnol.*, 2014, **9**, 687–692.
9 L. Protesescu, S. Yakunin, M. I. Bodnarchuk, F. Krieg, R. Caputo, C. H. Hendon, R. X. Yang, A. Walsh and M. V. Kovalenko, *Nano Lett.*, 2015, **15**, 3692–3696.
10 Q. A. Akkerman, V. D'Innocenzo, S. Accornero, A. Scarpellini, A. Petrozza, M. Prato and L. Manna, *J. Am. Chem. Soc.*, 2015, **137**, 10276–10281.
11 G. Nedelcu, L. Protesescu, S. Yakunin, M. I. Bodnarchuk, M. J. Grotevent and M. V. Kovalenko, *Nano Lett.*, 2015, **15**, 5635–5640.
12 B. R. Sutherland, A. K. Johnston, A. H. Ip, J. Xu, V. Adinolfi, P. Kanjanaboos and E. H. Sargent, *ACS Photonics*, 2015, **2**, 1117–1123.
13 P. Ramasamy, D. H. Lim, B. Kim, S. H. Lee, M. S. Lee and J. S. Lee, *Chem. Commun.*, 2016, **52**, 2067–2070.

14 F. Schwierz, *Nat. Nanotechnol.*, 2010, **5**, 487–496.
15 G. Konstantatos, M. Badioli, L. Gaudreau, J. Osmond, M. Bernechea, F. P. Garcia de Arquer, F. Gatti and F. H. Koppens, *Nat. Nanotechnol.*, 2012, **7**, 363–368.
16 Y. Lee, J. Kwon, E. Hwang, C. H. Ra, W. J. Yoo, J. H. Ahn, J. H. Park and J. H. Cho, *Adv. Mater.*, 2015, **27**, 41–46.
17 Y. Wang, Y. Zhang, Y. Lu, W. Xu, H. Mu, C. Chen, H. Qiao, J. Song, S. Li, B. Sun, Y.-B. Cheng and Q. Bao, *Adv. Opt. Mater.*, 2015, **3**, 1389–1396.
18 W. Guo, S. Xu, Z. Wu, N. Wang, M. M. Loy and S. Du, *Small*, 2013, **9**, 3031–3036.
19 H. Qiao, J. Yuan, Z. Xu, C. Chen, S. Lin, Y. Wang, J. Song, Y. Liu, Q. Khan and H. Y. Hoh, *ACS Nano*, 2015, **9**, 1886–1894.
20 K. T. Nguyen, D. Li, P. Borah, X. Ma, Z. Liu, L. Zhu, G. Gruner, Q. Xiong and Y. Zhao, *ACS Appl. Mater. Interfaces*, 2013, **5**, 8105–8110.
21 Z. Sun, Z. Liu, J. Li, G. A. Tai, S. P. Lau and F. Yan, *Adv. Mater.*, 2012, **24**, 5878–5883.
22 A. Kumar, S. Husale, A. K. Srivastava, P. K. Dutta and A. Dhar, *Nanoscale*, 2014, **6**, 8192–8198.
23 M. He, Y. Chen, H. Liu, J. Wang, X. Fang and Z. Liang, *Chem. Commun.*, 2015, **51**, 9659–9661.
24 S. H. Yu, Y. Lee, S. K. Jang, J. Kang, J. Jeon, C. Lee, J. Y. Lee, H. Kim, E. Hwang and S. Lee, *ACS Nano*, 2014, **8**, 8285–8291.
25 G. Konstantatos and E. H. Sargent, *Nat. Nanotechnol.*, 2010, **5**, 391–400.
26 J. P. Clifford, G. Konstantatos, K. W. Johnston, S. Hoogland, L. Levina and E. H. Sargent, *Nat. Nanotechnol.*, 2009, **4**, 40–44.
27 S. Keuleyan, E. Lhuillier, V. Brajuskovic and P. Guyot-Sionnest, *Nat. Photonics*, 2011, **5**, 489–493.

